• Basic Research •

Mesenchymal stem cells-derived exosomes ameliorate blue light stimulation in retinal pigment epithelium cells and retinal laser injury by VEGF-dependent mechanism

Guang-Hui He, Wei Zhang, Ying-Xue Ma, Jing Yang, Li Chen, Jian Song, Song Chen

Tianjin Eye Hospital; Tianjin Key Lab of Ophthalmology and Visual Science; Tianjin Eye Institute; Clinical College of Ophthalmology, Tianjin Medical University, Tianjin 300020, China

Co-first authors: Guang-Hui He and Wei Zhang

Correspondence to: Song Chen. Tianjin Eye Hospital; Tianjin Key Lab of Ophthalmology and Visual Science; Tianjin Eye Institute; Clinical College of Ophthalmology, Tianjin Medical University, No.4 Gansu Road, Tianjin 300020, China. chensong20@hotmail.com

Abstract

● **AIM:** To observe the effect of exosomes derived from human umbilical cord blood mesenchymal stem cells (hUCMSCs) on the expression of vascular endothelial growth factor-A (VEGF-A) in blue light injured human retinal pigment epithelial (RPE) cells and laser-induced choroidal neovascularization (CNV) in rats.

● **METHODS:** Exosomes were isolated from hUCMSCs and characterized by transmission electron microscope and Western blot. MSCs-derived exosomes were cultured with RPE cells exposed to blue light. The mRNA and protein expression of VEGF-A were determined by real time-polymerase chain reaction (PCR) and Western blot, respectively. Immunofluorescence assay was used for the detection of the expression level of VEGF-A. We injected different doses of MSCs-derived exosomes intravitreally to observe and compare their effects in a mouse model of laser-induced retinal injury. The histological structure of CNV in rats was inspected by hematoxylin-eosin (HE) staining and fundus fluorescein angiography. The expression of VEGF-A was detected by immunohistochemistry.

● **RESULTS:** Exosomes exhibited the typical characteristic morphology (cup-shaped) and size (diameter between 50 and 150 nm). The exosomes marker, CD63, and hUCMSCs marker, CD90, showed a robust presence. *In vitro*, MSCs-derived exosomes downregulated the mRNA(Exo-L: t=6.485, 7.959, 9.286; Exo-M: t=7.517, 10.170, 13.413; Exo-H: t=10.317, 12.234, 14.592, P<0.05) and protein (Exo-L: t=2.945, 4.477, 6.657; Exo-M: t=4.713, 6.421, 8.836; Exo-H: t=6.539, 12.194, 12.783; P<0.05) expression of VEGF-A in RPE cells after blue light stimulation. *In vivo*, we found that the MSCs-derived exosomes reduced damage, distinctly downregulated VEGF-A (Exo-H: t=0.957, 1.382; P<0.05), and gradually improved the histological structures of CNV for a better visual function (Exo-L: 0.346, Exo-M: 3.382, Exo-H: 8.571; P<0.05).

● **CONCLUSION:** MSCs-derived exosomes ameliorate blue light stimulation in RPE cells and laser-induced retinal injury *via* downregulation of VEGF-A.

● **KEYWORDS:** exosome; human umbilical cord mesenchymal stem cell; retinal pigment epithelial cell; choroidal neovascularization; vascular endothelial growth factor

INTRODUCTION

Age-related macular degeneration (AMD) continues to be the main cause of blindness in adults ≥65-year-old[1]. The development of choroidal neovascularization (CNV) in wet AMD patients usually leads to severe loss of vision. The current medical treatments are designed using the intravitreal injection of anti-vascular endothelial growth factor (anti-VEGF) drug, triamcinolone acetonide, photodynamic therapy, or laser photocoagulation on CNV membrane to prevent the progression of AMD[2]. However, if the retinal pigment epithelium (RPE) underlying the fovea is damaged severely, pharmacological treatment exerts limited effects on the best-corrected visual acuity (BCVA). The occurrence of drusen between Bruch membrane and RPE layer and the formation of CNV are the two pathological characteristics typical of AMD. Damage of visual function in AMD patients mainly results from the atrophy of RPE layer induced by the deposit of RPE metabolite and macular edema, histological destruction, and retinal hemorrhage due to CNV. The currently clinical therapies, such as photodynamic therapy and submacular surgery, are focused primarily on eliminating CNV[3-5].

Mesenchymal stem cells (MSCs) are originated from the embryonic mesoderm during embryonic development. MSCs are limited to bone marrow and adult connective tissues[6]. Moreover, they can clone and form adherent fibroblastic cells expressing the characteristic properties of cell surface markers. Since the cells are highly proliferative *ex vivo* and can differentiate along different cell lineages, they are considered as resources for transplantation and stem cell therapy[7]. In addition to soluble factors, exosomes are a sort of extracellular vesicles (EVs) sized approximately 100 nm (range, 30-120 nm) in diameter released from many different types of cells. Unlike other types of EVs, microvesicles (MVs) have different sizes (up to 2 μm) and are produced by various mechanisms[8]. Recent studies have confirmed a novel basis that exosomes may play crucial roles in providing intercellular communication[9]. MSC-derived exosomes (MSC-Exos) possess similar functions to MSCs. Despite the obvious advantages of MSC transplantation, the issues of allogeneic and heterologous immunological rejection concerns with respect to malignant transformation, and obstruction of small vessels continue to persist. These potential risks may be avoided by exosomes' administration. In addition, owing to the nanometer size, the exosomes can easily traverse the biological barriers and enter the target organs[10].

Previously, we demonstrated that neural stem cells originating from MSCs exhibit a neuroprotective effect by increasing the number of surviving retinal ganglion cells and notably reduce the progression of diabetic retinopathy (DR)[11]. The transplantation of MSC-Exos could be a novel choice for the treatment of AMD. In the present study, we investigated if MSC-Exos could ameliorate the blue light stimulation in RPE cells and retinal laser injury.

MATERIALS AND METHODS

Cell Culture and Isolation and Characterization of Exosomes
The study was approved by Tianjin Medical University Medical Ethics Committee and conducted in accordance with the Declaration of Helsinki, including current revisions and with Good Clinical Practice guidelines. We isolated and differentiated the umbilical cord blood mesenchymal stem cells (UCMSCs) according to the previously published protocol[10]. Briefly, the morphology of the human UCMSCs (hUCMSCs) was uniformly spindle-shape with a racial or spiral-shaped arrangement. Flow cytometric studies indicate that the MSCs exhibited a characteristic immune phenotype; CD73, CD90, and CD105 were highly expressed, while CD11b, CD19, CD34, CD45, and HLA-D were weakly expressed.

Supernatants of MSCs at passage 3 cultured in fetal bovine serum (FBS)-free medium were centrifuged at 200, 2000, and 10 000 ×g, sequentially, to remove the cells and cell debris, followed by centrifugation at 110 000 ×g for 2h. After washing two times, the pellet was resuspended in PBS. The morphology

of exosomes were observed by scanning electron microscopy, and the surface markers of exosomes were identified by proteomic analysis.

Cell Model Preparation ARPE-19 cells (immortalized human RPE cells, passage 30-50; Biorega, China) were cultivated in DMEM supplemented with 10% exosome-depleted FBS and 1% penicillin-streptomycin agents (Santa Cruz Biotechnology, Santa Cruz, CA, USA), in 75 mL flasks. The ARPE-19 cells were divided into several groups randomly: normal control group with no treatment, model group prepared for blue light irradiation, model group treated with MSC-Exos. The cells of MSC-Exos-treated group were treated with different concentrations of exosomes (Exo-L: 25 μg/mL, Exo-M: 50 μg/mL, and Exo-H: 75 μg/mL) for 8, 16, and 24h. For blue light irradiation of RPE cells, we employed a 3×3 array of blue LEDs (XL amp XP-E royal blue; Cree, Durham, NC, USA). The spectral measurements of LED spectra showed a peak wavelength of 448 nm with 2000±500 lx. Subsequently, the cells were treated with radiation from a distance of 35 cm within a cell culture incubator for 12h. In this setting, the cells were exposed to radiation treatment at 0.8 mW/cm^2 as measured using a power meter (Coherent, Santa Clara, CA, USA). The results showed that the radiation treatment did not have any effect on the temperature of the cell medium.

Real-time Quantitative Polymerase Chain Reaction
Following MSCs-Exos treatment, total RNA was obtained from ARPE-19 cells using RNeasy Micro/Mini Kits (Invitrogen, CA, USA) according to the manufacturer's instructions. mRNA was reverse transcribed (cDNA synthesis) using GoTaq polymerase chain reaction (PCR) master mix (Invitrogen) under the following reaction conditions: 94℃ for 30s, 62℃ for 30s, and 72℃ for 1min. Then, the cDNA was subjected to real-time quantitative PCR using SYBR Green Supermix (Invitrogen) in a Roche 234 Light Cycler 480 PCR System. The primer sequences were as follows: GAPDH: Fwd 5'-ATCCCATCACCATCTTCC-3'; Rev 5'-ATCACGCCACAGTTTCC-3'; VEGFR: Fwd 5'-GGCTGTTCTCGCTTCG-3'; Rev 5'-TGTCCACCAGGG TCTCG-3'. Each sample was analyzed in triplicates, and a cycle threshold (Ct) value of transcripts was determined in the exponential phase using Light Cycler software 4.0. Finally, the fold-change in the mRNA levels was determined by the $2^{-\triangle\triangle Ct}$ method.

Immunocytochemistry Immunocytochemistry was performed when the ARPE-19 cells were grown as monolayers on transwell plates. Subsequently, the cells were fixed in 4% paraformaldehyde, washed, and probed with polyclonal antibody to anti-VEGF-A (1:200; Shenyang Wanlei, China) in blocking solution, followed by incubation with secondary antibody. None of the immunohistochemistry experiments

included a primary antibody control. The staining was examined *via* a fluorescence microscope (Zeiss, USA) equipped with a digital camera.

Western Blot ARPE-19 cells were collected by trypsinization, washed with PBS, and resuspended in lysis buffer [50 mmol/L Tris-HCl (pH 7.4), 150 mmol/L NaCl, 1 mmol/L EDTA, 1% Triton X-100] supplemented with protease and phosphatase inhibitors (Thermo Scientific, Rockford, IL, USA). SDS-PAGE and Western blot were performed according to the standard methods. The antibodies used for probing the membrane included anti-VEGF-A or GADPH (Shenyang Wanlei, China). The immunoreactive bands were imaged and quantified using the LiCOR Odyssey system (Zeiss, Germany).

Animal Model Preparation Brown Norway (BN) male rats 12-week were purchased from Tianjin Medical University. The care and use of all animals conformed to the regulations in the ARVO Statement for the Use of Animals in Ophthalmic and Vision Research and approved by the Laboratory Animal Care and Use Committee of the Tianjin Medical University. The rats were randomly divided into several groups: normal control group with no treatment (*n*=15), model group prepared for retinal laser injury models (*n*=15), animal model transplanted with PBS following model preparation (*n*=15), animal model transplanted with different concentrations of MSCs-Exos (Exo-L: 1.0 μL of 50 μg/mL, *n*=15; Exo-M: 2.0 μL of 50 μg/mL, *n*=15; Exo-H: 3.0 μL of 50 μg/mL, *n*=15).

The mice were anesthetized by chloral hydrate at 500 mg/kg body weight intraperitoneally, and then, the pupil was dilated with 0.5% tropicamide. A krypton laser (NOVUS OMNI, Coherent, USA; wavelength, 577 nm; power, 200 mW; exposure time, 100ms; diameter, 100 μm) was used to generate 8 laser spots on the left retina of each mouse using glass slide. Each laser spot was distanced >200 μm from others while avoiding the major vessels. For treatment, 5 μL PBS alone, MSCs-Exos at the concentration of 50 μg/mL were intravitreally injected immediately after the laser injury. The right eyes served as normal controls.

Histological Analysis The eyes, obtained from the animal models, were fixed, dehydrated, and embedded in paraffin. HE staining and immunohistochemistry were performed on 4 μm-thick serial coronal sections of the retinas. The sections at the centers of laser spots were selected from continuous slices. After antigen retrieval, 5% bovine serum albumin (BSA) was incubated with the slices to block the non-specific binding. The sections were incubated with an antibody against mouse VEGF-A (Shenyang Wanlei, China) according to the manufacturer's instructions. Diaminobenzidine substrate (Zhong Shan Jin Qiao, China) was used for color development following the manufacturer's protocol and observed by light microscopy. The damaged retina was defined as the area in which, the normal cytoarchitectural alters in any retinal layer

could be distinguished, according to the method described previously. The quantification of VEGF-A immunostaining was calculated using a computer imaging analysis system as follows: the proportion of the area occupied by the brown staining in the retinal tissue.

Fundus Fluorescein Angiography The rats were anesthetized, and injected peritoneally with 10% fluorescein sodium (0.5 mL/kg). Rats were fixed on a slit-lamp delivery system, and the ocular fundus was recorded consecutively by fundus camera system (Zeiss, USA). Fundus fluorescein angiography (FFA) was tested 14d after injection in each experimental group.

Statistical Analysis The data were presented as mean±SEM. All experiments were repeated at least three times. The data were compared by one-way ANOVA. *P*<0.05 was considered statistically significant. All analyses were performed using a statistical software package (SPSS 13.0; SPSS Inc., Chicago, IL, USA).

RESULTS

Isolation and Characterization of MSCs-derived Exosomes Exosomes shed by MSCs were isolated with a series of centrifugation and ultracentrifugation steps. Then, the identity of the exosomes was confirmed by electron microscopy. The exosomes were observed in the extracellular medium of MSCs (Figure 1). The exosomes exhibited the typical characteristic morphology (cup-shaped) and size (diameter between 50 and 150 nm). The exosomes were further characterized by Western blot in the presence of exosomal protein marker, CD63, and the MSC protein marker, CD90 (Figure 2).

MSCs-derived Exosomes Downregulate VEGF-A Expression in ARPE-19 Cells To determine whether VEGF-A downregulation was observed in RPE cells in response to MSCs-Exos treatment, RT-PCR, immunohistochemistry, and Western blotting were used to assess the expression of VEGF-A. Consequently, the mRNA levels of VEGF-A in RPE cells were evaluated in response to MSCs-Exos treatment and were found to be markedly decreased in MSCs-Exos-treated cells at 8, 16, and 24h as compared to the model group (Exo-L: *t*=6.485, 7.959, 9.286; Exo-M: *t*=7.517, 10.170, 13.413; Exo-H: *t*=10.317, 12.234, 14.592, *P*<0.05; Figure 3). The mRNA levels of VEGF-A decreased consistently with the passage of time and the increasing concentration of MSCs-Exos (*F*=6.478, 8.872, 23.704, *P*<0.05). In addition, the protein levels of VEGF-A were also found to be markedly decreased in MSCs-Exos-treated cells as compared to the model group (Exo-L: *t*=2.945, 4.477, 6.657; Exo-M: *t*=4.713, 6.421, 8.836; Exo-H: *t*=6.539, 12.194, 12.783, *P*<0.05; Figure 4). The protein levels of VEGF-A decreased consistently with the passage of time and the increasing concentration of MSCs-Exos (*F*=3.980, 11.148, 45.496, *P*<0.05). Similarly, immunohistochemistry showed positive staining for VEGF-A in MSCs-Exos-treated cells as compared to the model group (Figure 5). These results
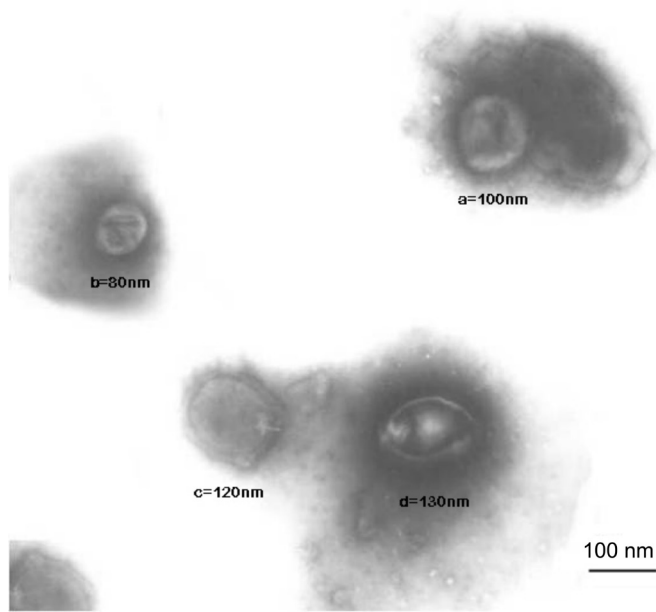
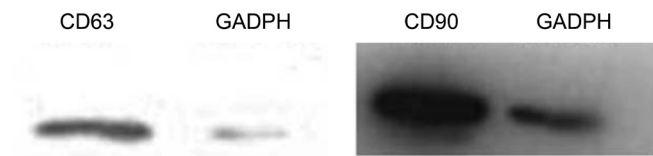**Figure 1 Exosomes released from MSCs exhibited the classical morphology and size (50-150 nm).**

Figure 2 Expression of CD63 and CD90 proteins in exosomes detected by Western blot.
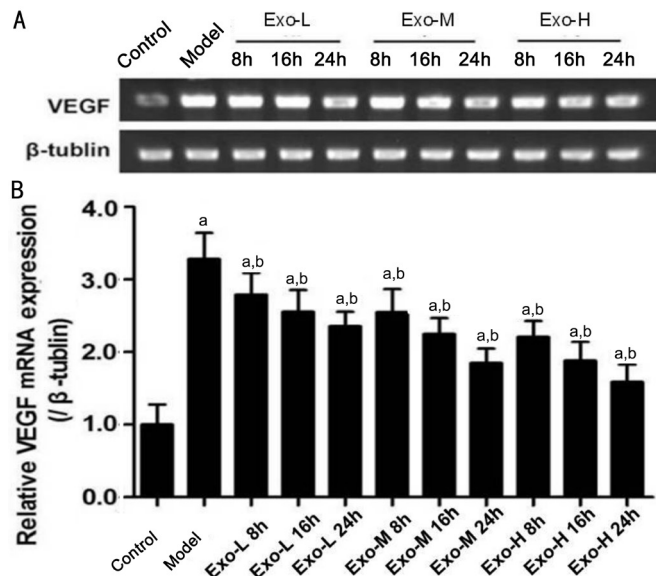

Figure 3 VEGF mRNA expression A: A representative RT-PCR was shown; B: VEGF-A mRNA levels were found to be markedly decreased in MSCs-Exos-treated cells at 8, 16, and 24h as compared to the model group. The mRNA levels of VEGF-A decreased consistently with the passage of time and the increasing concentration of MSCs-Exos. [a]$P<0.05$ compared with control; [b]$P<0.05$ compared with model.

confirmed that MSCs-Exos comprise the critical mechanism underlying VEGF-A downregulation in the current study.
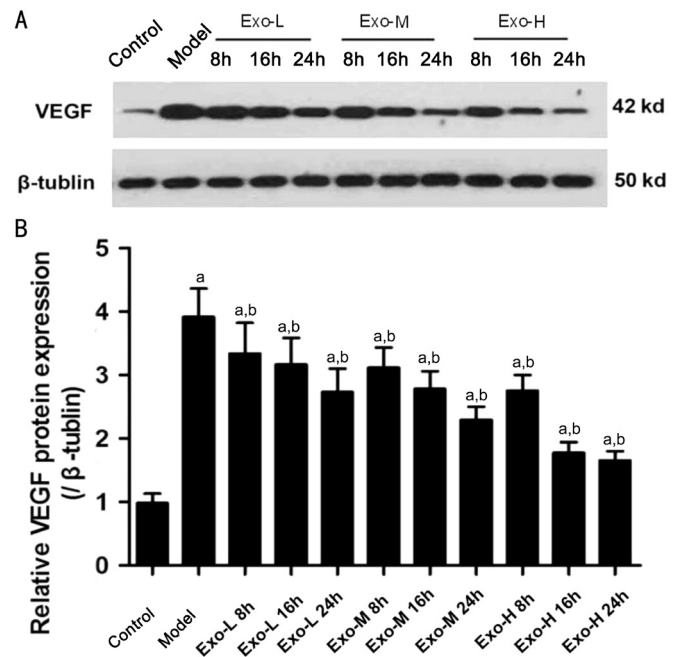
Figure 4 Western blot analysis of VEGF A: A representative Western blot was shown; B: VEGF-A protein levels were found to be markedly decreased in MSCs-Exos-treated cells as compared to the model group. The protein levels of VEGF-A decreased consistently with the passage of time and the increasing concentration of MSCs-Exos. [a]$P<0.05$ compared with control; [b]$P<0.05$ compared with model.
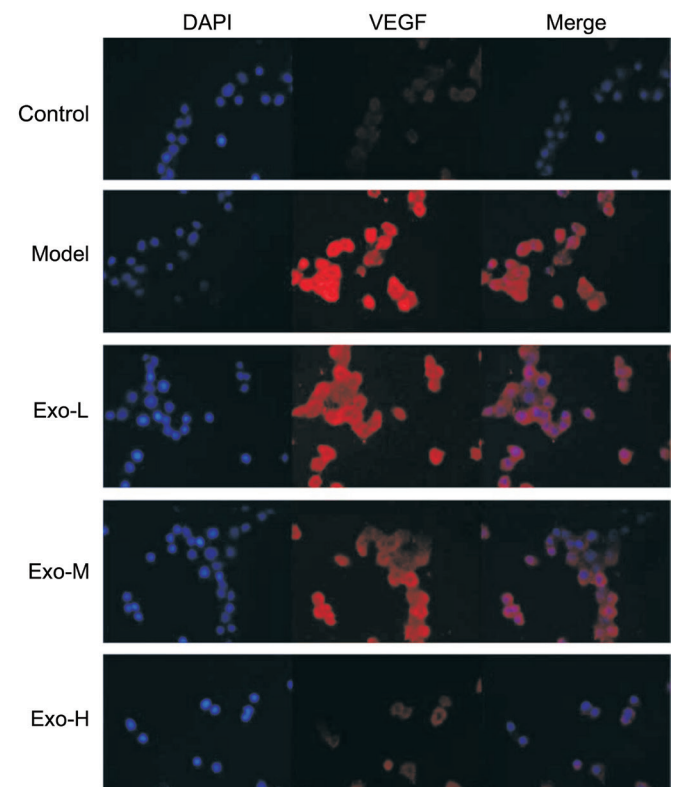

Figure 5 VEGF expression was observed under a fluorescence microscope after immunostaining DAPI was used for staining the nuclei. Immunohistochemistry showed positive staining of VEGF-A in MSCs-Exos-treated cells as compared to the model group.

Histopathology The structure of retina was continuous with normal capillary structure in the control group (Figure 6A).
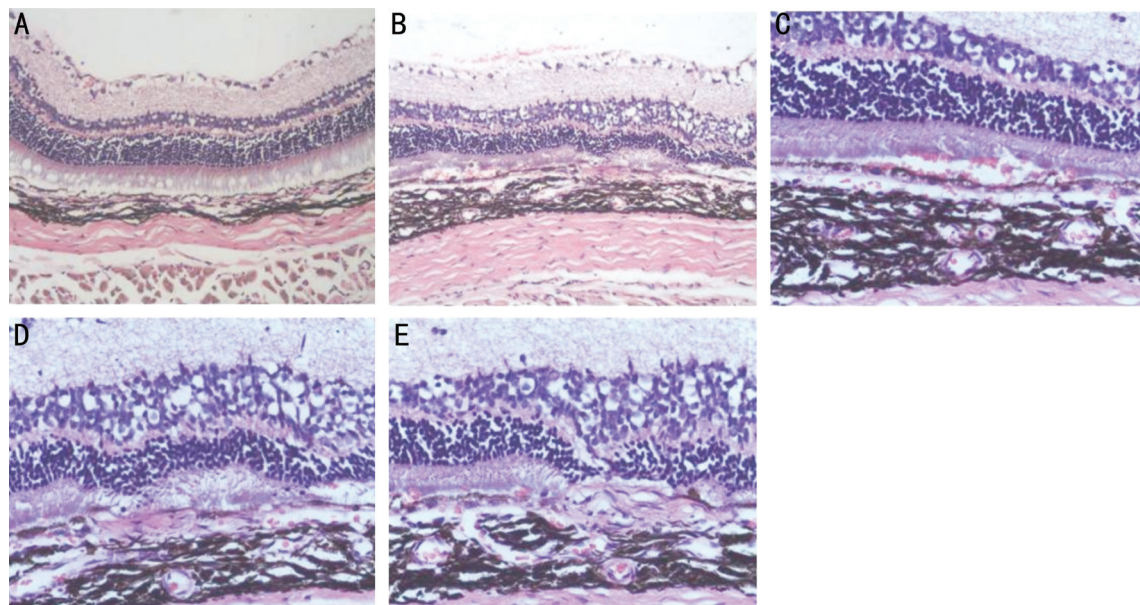
Figure 6 Retinal HE staining A: The structure of the retina was continuous and its capillary structure normal in control group; B: Bruch's membrane and RPE layer were destroyed at the center of laser lesions 14d post-laser photocoagulation; C: Neovascular with wide lumens stretched from the choroid into the subretinal space 21d after laser photocoagulation; D: Treatment with MSCs-derived exosomes attenuated the development of CNV 14d after laser photocoagulation; E: Fibroblasts and collagen fibers were reduced, and large sets of vascular channels were not observed in the subretinal space 21d after laser photocoagulation.

Table 1 Expression of VEGF-A n=5

Groups	Day 7	Day 14	Day 21	F	P
Model	9.91±0.89	29.16±1.32	40.26±1.90	575.675	<0.001
Model with PBS	10.11±0.85	28.25±0.51	39.87±0.89	1901.37	<0.001
Exo-L	9.46±0.62	20.83±1.24[a,b]	20.00±0.84[a,b]	229.351	<0.001
Exo-M	7.98±0.30[a,b,c]	17.69±0.58[a,b,c]	16.31±0.62[a,b,c]	510.537	<0.001
Exo-H	5.80±0.88[a,b,c,d]	12.59±0.96[a,b,c,d]	10.58±0.96[a,b,c,d]	69.713	<0.001
F	29.282	258.414	742.182		
P	<0.001	<0.001	<0.001		

[a]P<0.05 compared with model; [b]P<0.05 compared with model with PBS; [c]P<0.05 compared with Exo-L; [d]P<0.05 compared with Exo-H.

The Bruch membrane and RPE layer were disrupted in the center of laser burns, and the layer of choroid was destroyed within the laser burn 14d post-laser photocoagulation (Figure 6B). Retinal edema was found, and newly formed vessels extended from the choroid into the subretinal space 21d after laser photocoagulation (Figure 6C). Treatment with MSCs-Exos attenuated the development of CNV 14d after laser photocoagulation (Figure 6D). As a result, fibroblasts and collagen fibers were reduced. In addition, large sets of vascular channels were not observed in the subretinal space 21d after laser photocoagulation (Figure 6E).

The expression of VEGF-A increased gradually in the rats of model group at 14 and 21d post-laser photocoagulation. However, the expression of VEGF-A decreased when treated with MSCs-Exos (P<0.05). The three treated groups (Exo-L, Exo-M, and Exo-H) showed a decreased protein expression of VEGF-A at 14 and 21d after laser photocoagulation. Also, we found that the VEGF-A protein expression in the Exo-H group

was significantly lower than that in the other treated groups (t=0.957, 1.382; P<0.05; Table 1).

Fundus Fluorescein Angiography The examination of FFA showed large areas of CNV at Bruch membrane rupture sites at 14d after laser photocoagulation (Figure 7A). The results indicated a successful establishment of the CNV model. Treatment with MSCs-Exos attenuated the leakages as compared to the model group (Exo-L: 0.346, Exo-M: 3.382, Exo-H: 8.571; P<0.05; Figure 7B-7D). We found that the leakages in the Exo-H group were prominently lower than that in the Exo-L group (5.698, P<0.05). The Exo-H group had a remarkable inhibitory effect on the leakages in all the three treated groups.

DISCUSSION

The present findings indicated that MSCs-Exos ameliorate the blue light stimulation in RPE cells and laser-induced retinal injury *via* the downregulation of VEGF-A. Considering the physiological function and location, the RPE cells are
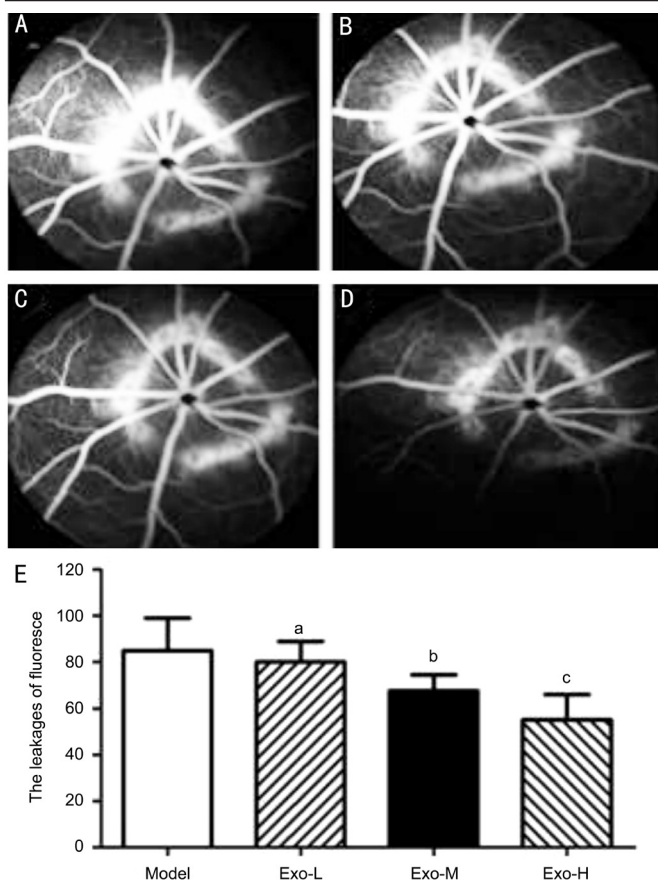
Figure 7 Retinal FFA analysis A: The examination of FFA showed large areas of CNV at Bruch membrane rupture sites at 14d after laser photocoagulation; B-D: Treatment with MSCs-Exos attenuated the leakages as compared to the model group with PBS. Exo-H group had a remarkable inhibitory effect on the leakages in all the three treated groups; E: The leakages of fluoresce in 14d after laser photocoagulation. [a]Compared with model $P<0.05$, [b]Compared with Exo-L $P<0.05$, [c]Compared with Exo-M $P<0.05$.

exposed to a variety of reactive oxygen species (ROS); thus, the protection of RPE cells from light damage may be an ideal strategy for the treatment of AMD[12]. We used blue light to induce VEGF expression in ARPE-19 cells. The blue light-induced oxidative stress is a typical model that can detect the expression of VEGF in RPE cells sensitively[12]. Moreover, the exposure to light is related to the occurrence and development of AMD putatively through the pathology of VEGF mechanism[13]. Although the blue light illumination induced ROS generation in RPE cells and increased their production in mitochondria, a positive correlation was established between light-induced oxidation and age[14]. Western blot and RT-PCR were employed for the quantification of VEGF expression. We observed that blue light radiation treatment could induce VEGF expression remarkably. These results suggested that blue light could induce VEGF expression in ARPE-19 cells and that it could be used for stimulating the disease model in the current study.

Presently, MSCs have become a promising source of stem cell regeneration medicine and are considered superior to other types of stem cells because of convenient isolation, long-term cryopreservation, *ex vivo* expansion, easy genetic manipulation, and some ethical and legal concerns[15]. Although these cells have been conventionally withdrawn from bone marrow, umbilical cord, and associated tissues, such as artery, umbilical cord vein, and placenta, they have been recently speculated as an alternative source of MSCs[16]. Therefore, hUCMSCs are expected to become cellular candidates for stem cell therapy and transplantation. MSCs are capable of secreting exosomes as reported previously, and exosome markers have been associated with AMD (during the discovery of drusen)[17]. Recent studies have found that several types of cell, including MSCs, can affect the adjacent cells by the release of exosomes[18]. Moreover, the MSCs-Exos seem to reduce the leakage of the vessel in a model of AMD, whereas RPE-derived exosomes do not prevent the leakage of new blood vessels[19]. Consequently, another group showed that MSCs-Exos could inhibit the neovascularization by inhibiting NF-β signaling[20]. Furthermore, exosomes are known to transfer functional miRNAs, proteins, and mRNAs to recipient cells[21]. The *in vitro* experiments demonstrated that exosomes harbor the potential to downregulate the expression of VEGF in RPE cells. These results support the critical role of VEGF in the pathogenesis of retina damage, thereby suggesting that MSC-Exos exert their protective effect *via* VEGF regulation.

The laser-induced retina injury model is widely used in the study of retinal injury. In the current study, the power, wavelength, and exposure time of the laser were controlled to avoid damage to the Bruch membrane. Moreover, eight laser spots were generated on each retina, such that each laser spot was at least two-spot diameters away from the others. The number of laser spots not only made it easier to obtain sufficient histological data from an equivalent number of samples but could also detect the changes in the retinal function based on electroretinogram evaluation. Herein, separate lesions spaced by normal retina could also be observed under the microscope with eight laser spots generated in one mouse eye, indicating that this mouse model was suitable for the study of the retinal injury. Previous studies have shown that laser injury ablates the RPE and causes damage to the photoreceptor, resulting in the release of pro-vascular mediators, such as VEGF[22-23]. We found that the expression of VEGF was increased at an early stage post-injury, which was strongly inhibited by MSC-Exos, suggesting a key role in the inhibition of VEGF by exosomes. Thus, we speculated that MSC-Exos might be optimal candidates for intravitreal injection, which could potentially overcome the obstacles and risks related to stem cell transplantation therapy, such as possible long-term pathological differentiation, vitreous opacities, and poor preservation[24].

In conclusion, we demonstrated that MSC-Exos exerted beneficial effects on the repair of blue light-induced retinal laser injury. The downregulation of VEGF expression might be influenced by vital proteins or RNAs encapsulated in MSC-Exos. These results suggested that the transplantation of MSC-Exos might act as a putative therapeutic tool to protect the retina. In future studies, we will examine the safety of this procedure in large animal models that closely mimic the human eye in order to better understand the direct relationship between the constituents of MSC-Exos and VEGF regulation.

ACKNOWLEDGEMENTS

Conflicts of Interest: He GH, None; **Zhang W,** None; **Ma YX,** None; **Yang J,** None; **Chen L,** None; **Song J,** None; **Chen S,** None.

REFERENCES

1 Mahmoudzadeh R, Heidari-Keshel S, Lashay A. Schwann cell-mediated preservation of vision in retinal degenerative diseases via the reduction of oxidative stress: a possible mechanism. *Med Hypothesis Discov Innov Ophthalmol* 2016;5(2):47-52.

2 Brown GC, Brown MM, Lieske HB, Turpcu A, Rajput Y. The comparative effectiveness and cost-effectiveness of ranibizumab for neovascular macular degeneration revisited. *Int J Retina Vitreous* 2017;3:5.

3 Wilde C, Poostchi A, Mehta RL, MacNab HK, Hillman JG, Vernon SA, Amoaku WM. Prevalence of age-related macular degeneration in an elderly UK Caucasian population-The Bridlington Eye Assessment Project: a cross-sectional study. *Eye (Lond)* 2017;31(7):1042-1050.

4 Bobis-Wozowicz S, Kmiotek K, Sekula M, Kedracka-Krok S, Kamycka E, Adamiak M, Jankowska U, Madetko-Talowska A, Sarna M, Bik-Multanowski M, Kolcz J, Boruczkowski D, Madeja Z, Dawn B, Zuba-SurmaEK. Human Induced Pluripotent Stem Cell-Derived Microvesicles Transmit RNAs and Proteins to Recipient Mature Heart Cells Modulating Cell Fate and Behavior. *Stem Cells* 2015;33(9):2748-2761.

5 Wang Y, Fu B, Sun X, Li D, Huang Q, Zhao W, Chen X. Differentially expressed microRNAs in bone marrow mesenchymal stem cell-derived microvesicles in young and older rats and their effect on tumor growth factor-β1-mediated epithelial-mesenchymal transition in HK2 cells. *Stem Cell Res Ther* 2015;6:185.

6 He J, Wang Y, Lu X, Zhu B, Pei X, Wu J, Zhao W. Micro-vesicles derived from bone marrow stem cells protect the kidney both in vivo and in vitro by microRNA-dependent repairing. *Nephrology* (*Carlton*) 2015;20(9):591-600.

7 Jarmalavičiūtė A, Tunaitis V, Pivoraitė U, Venalis A, Pivoriūnas A. Exosomes from dental pulp stem cells rescue human dopaminergic neurons from 6-hydroxy-dopamine-induced apoptosis. *Cytotherapy* 2015;17(7):932-939.

8 Phinney DG, Di Giuseppe M, Njah J, Sala E, Shiva S, St Croix CM, Stolz DB, Watkins SC, Di YP, Leikauf GD,Kolls J, Riches DW, Deiuliis G, Kaminski N, Boregowda SV, McKenna DH, Ortiz LA. Mesenchymal stem cells use extracellular vesicles to outsource mitophagy and shuttle microRNAs. *Nat Commun* 2015;6:8472.

9 Zhang W, Wang Y, Kong J, Dong M, Duan H, Chen S. Therapeutic efficacy of neural stem cells originating from umbilical cord-derived mesenchymal stem cells in diabetic retinopathy. *Sci Rep* 2017;7(1):408.

10 Chen S, Zhang W, Wang JM, Duan HT, Kong JH, Wang YX, Dong M, Bi X, Song J. Differentiation of isolated human umbilical cord mesenchymal stem cells into neural stem cells. *Int J Ophthalmol* 2016;9(1):41-47.

11 Iannaccone A, Giorgianni F, New DD, *et al*. Circulating autoantibodies in age-related macular degeneration recognize human macular tissue antigens implicated in autophagy, immunomodulation, and protection from oxidative stress and apoptosis. *PLoS One* 2015;10(12):e0145323.

12 Blasiak J, Petrovski G, Veréb Z, Facskó A, Kaarniranta K. Oxidative stress, hypoxia, and autophagy in the neovascular processes of age-related macular degeneration. *Biomed Res Int* 2014;2014:768026.

13 Brandstetter C, Patt J, Holz FG, Krohne TU. Inflammasome priming increases retinal pigment epithelial cell susceptibility to lipofuscin phototoxicity by changing the cell death mechanism from apoptosis to pyroptosis. *J Photochem Photobiol B* 2016;161:177-183.

14 Kang JH, Choung SY. Protective effects of resveratrol and its analogs on age-related macular degeneration in vitro. *Arch Pharm Res* 2016;39(12):1703-1715.

15 Wang Y, Zhang L, Li Y, Chen L, Wang X, Guo W, Zhang X, Qin G, He SH, Zimmerman A, Liu Y, Kim IM, Weintraub NL, Tang Y. Exosomes/microvesicles from induced pluripotent stem cells deliver cardioprotective miRNAs and prevent cardiomyocyte apoptosis in the ischemic myocardium. *Int J Cardiol* 2015;192:61-69.

16 Kang T, Jones TM, Naddell C, Bacanamwo M, Calvert JW, Thompson WE, Bond VC, Chen YE, Liu D. Adipose-derived stem cells induce angiogenesis via microvesicle transport of miRNA-31. *Stem Cells Transl Med* 2016;5(4):440-450.

17 Kang GY, Bang JY, Choi AJ, Yoon J, Lee WC, Choi S, Yoon S, Kim HC, Baek JH, Park HS, Lim HJ, ChungH. Exosomal proteins in the aqueous humor as novel biomarkers in patients with neovascular age-related macular degeneration. *J Proteome Res* 2014;13(2):581-595.

18 Kwan KM. Coming into focus: the role of extracellular matrix in vertebrate optic cup morphogenesis. *Dev Dyn* 2014;243(10):1242-1248.

19 Phillips MJ, Perez ET, Martin JM, Reshel ST, Wallace KA, Capowski EE, Singh R, Wright LS, Clark EM, Barney PM, Stewart R, Dickerson SJ, Miller MJ, Percin EF, Thomson JA, Gamm DM. Modeling human retinal development with patient-specific induced pluripotent stem cells reveals multiple roles for visual system homeobox 2. *Stem Cells* 2014;32(6):1480-1492.

20 Atienzar-Aroca S, Flores-Bellver M, Serrano-Heras G, Martinez-Gil N, Barcia JM, Aparicio S, Perez-Cremades D, Garcia-Verdugo JM, Diaz-Llopis M, Romero FJ, Sancho-Pelluz J. Oxidative stress in retinal pigment epithelium cells increases exosome secretion and promotes angiogenesis in endothelial cells. *J Cell Mol Med* 2016;20(8):1457-1466.

21 Knickelbein JE, Liu B, Arakelyan A, Zicari S, Hannes S, Chen P, Li Z, Grivel JC, Chaigne-Delalande B, Sen HN, Margolis L, Nussenblatt RB. Modulation of immune responses by extracellular vesicles from retinal pigment epithelium. *Invest Ophthalmol Vis Sci* 2016;57(10): 4101-4107.

22 Hayashi R, Ishikawa Y, Sasamoto Y, Katori R, Nomura N, Ichikawa T, Araki S, Soma T, Kawasaki S, Sekiguchi K, Quantock AJ, Tsujikawa M, Nishida K. Co-ordinated ocular development from human iPS cells and recovery of corneal function. *Nature* 2016;531(7594):376-380.

23 Gangalum RK, Bhat AM, Kohan SA, Bhat SP. Inhibition of the expression of the small heat shock protein αb-crystallin inhibits exosome secretion in human retinal pigment epithelial cells in culture. *J Biol Chem* 2016;291(25):12930-12942.

24 Aboul Naga SH, Dithmer M, Chitadze G, Kabelitz D, Lucius R, Roider J, Klettner A. Intracellular pathways following uptake of bevacizumab in RPE cells. *Exp Eye Res* 2015;131:29-41.